



Cite this: *Chem. Soc. Rev.*, 2017, 46, 7306

Synthesis and reduction of large sized graphene oxide sheets

Lei Dong,^a Jieun Yang,^b Manish Chhowalla*^b and Kian Ping Loh *^a

Graphene oxide (GO) can be considered as one of the most visible outcomes of graphene research in terms of large scale production and commercialization prospects. Although GO can be easily prepared by oxidation–exfoliation of graphite in agitated solutions, the size of these sheets is generally limited due to fragmentation along fault lines during chemical oxidation and exfoliation in agitated solutions. In this account, we discuss recent strategies which have been developed for the preparation of large sized graphene oxide (LGO) sheets with lateral sizes $>10\ \mu\text{m}$, using chemically expanded graphite as the starting material. LGO has a much lower density of defects than GO prepared using the conventional Hummers' method and can be readily transformed into graphene by chemical reduction. In addition, the unique advantages of using LGO sheets as a performance enhancer are discussed. Finally, this review also discusses recent advances in the chemical and electrochemical reduction of graphene oxide.

Received 30th June 2017

DOI: 10.1039/c7cs00485k

rsc.li/chem-soc-rev

1. Introduction

Graphene oxide (GO), the oxygen-functionalized and solution processable form of graphene, has emerged as an important additive and performance enhancement material in composites, and as a structural reinforcement agent in fibers,¹ energy storage devices,² molecular sieves,³ and liquid-crystal optical materials.⁴ Due to its 2-D nature and tunable functionalities, GO can be stacked in a layer by layer manner to form macroscopic self-assembled films. When GO is processed into a lamellar film with a lateral dimension larger than that of a single flake, colligative properties can arise, such as inter-planar nanochannels for ultrafiltration,³ liquid crystal-like light-scattering properties⁴ and so on. The mean size of GO sheets has a major influence on their colligative properties. Here, we define large sized graphene oxide (LGO) sheets as GO sheets with lateral dimensions $>10\ \mu\text{m}$. An LGO network contains fewer inter-sheet junctions than its small graphene oxide (SGO) counterpart; thus films made from LGO show better electrical and thermal conductivities and higher efficiency in load transfer (Fig. 1).^{5–7} Many properties of GO-based materials are limited by the small flake size of GO. For example, when GO is stacked to form molecular sieves or filtration membranes, the membranes assembled from small sized GO flakes are disadvantaged by leaky paths due to boundaries and weak mechanical properties.⁸

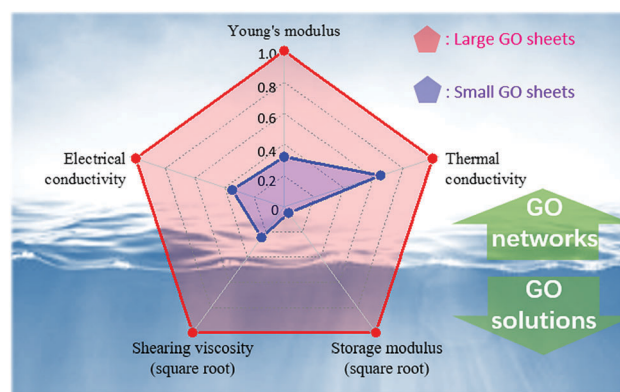


Fig. 1 Schematic illustration of the size-dependent properties (normalized) of GO based solutions or networks, where electrical conductivity,⁶ Young's modulus⁶ and thermal conductivity¹³ are obtained from GO films and shearing viscosity¹¹ and storage modulus¹¹ are obtained from GO aqueous dispersions.

In addition, it is easier to get a well-ordered microstructure from LGO dispersion compared to SGO due to its nematic liquid crystallinity and rheological properties (*e.g.* its higher viscosity, higher modulus and lower critical gel concentration) (Fig. 1).^{9–12} Increasingly, the limiting factors in devices and systems made from solution-derived graphene are traced to the limited size of the flakes; therefore, a better way for exfoliating graphite has to be developed to optimize the yield and size of the exfoliated GO.

Although GO sheets can be easily prepared by oxidation–exfoliation of graphite in agitated solutions, it is generally difficult to obtain LGO sheets in high yield. Single layer GO sheets are vulnerable to mechanical agitation caused by ultrasonic waves,

^a Department of Chemistry and Center for Advanced 2D Materials, National University of Singapore, 3 Science Drive 3, 117543, Singapore. E-mail: chmlhkp@nus.edu.sg

^b Rutgers University, Department of Materials Science and Engineering, Piscataway, NJ 08854, USA. E-mail: manish1@soe.rutgers.edu

stirring and even hand-shaking, and crack easily along the in-plane direction.^{11,14} During the exfoliation of graphite, harsh conditions (*e.g.* excessive oxidizer and high reaction temperature) are typically applied to complete the diffusion-controlled oxidation process, this exacerbates crack formation in GO sheets.^{14–17} In this account, recent progress in the preparation of LGO is summarized, with an emphasis on how to optimize yield and sheet size. In addition, the unique advantages of using LGO sheets as a performance enhancer are discussed. We also discuss recent progress in the reduction of GO to achieve properties that approach those of graphene.

2. Solution-processed preparation of LGO

As shown in Fig. 2a, the chemical methods for synthesizing GO generally involve two steps: preparation of graphite oxide *via* chemical oxidation, followed by the exfoliation of graphite oxide *via* mechanical agitation. In most cases, the two steps occur simultaneously because of continuous mechanical stirring throughout the whole process.^{19–22} Various strategies that aim at minimizing the cracking of GO sheets by making the reaction conditions less vigorous have been attempted. However, the yield of LGO is low in most cases, despite a high energy consumption in the synthesis processes.^{5,6,15,21,23–28} The pre-treatment of graphite also affects the final size of GO obtained.^{11,15,24,29} The oxidation of graphite is a kinetically-driven process in which the oxidation rate depends primarily on the diffusion of the oxidizer and not on the reactivity of carbon atoms.¹⁸ Experimental observation reveals heterogeneous, time-dependent oxidation patterns where the oxidizer propagates from the edge to the center within sub-nanometer interlayer channels of graphite (Fig. 2b).¹⁸ Therefore, an excessive amount of oxidizer and harsh reaction conditions are applied to prevent incomplete oxidation or extremely long reaction times.^{19–22,30,31} For example, Hummers' method used in conventional GO synthesis requires more than 6 weight equivalents of KMnO_4 oxidizer (relative to the weight of graphite) and a reaction temperature over $90\text{ }^\circ\text{C}$ during the first

water addition step.^{19,25} During the oxidation process, the epoxy groups (C–O–C) that are created introduce local distortion on the basal plane due to its sp^3 -hybridized geometry, which tends to stretch and break the underlying C–C bond.¹⁶ The epoxy groups on the GO plane have a tendency to aggregate into chain-like fault lines due to proximity-enhanced reactivity (Fig. 2c).³² As a consequence, GO sheets with a high concentration of oxygen groups have a strong tendency to disintegrate into smaller fragments.^{14–16}

There have been attempts to reduce the oxidation-induced cutting.^{5,15,23} For example, a two-step strategy (preoxidation–oxidation) reduced the reaction temperature to $35\text{ }^\circ\text{C}$, yielding LGO sheets with a mean area $>112\text{ }\mu\text{m}^2$.²⁴ A lower oxidizer loading facilitates the preparation of LGO, but this comes at a price of lower yields and longer times needed for size-fractionation.^{13,27} Mechanical agitation, which is applied to overcome the van der Waals forces between the GO sheets, inevitably creates collateral damage by fragmenting the GO sheets. Indeed, shaking alone can cut the GO sheets into small pieces (*e.g.* the percentage of LGO sheets reduces from $\sim 42\%$ to 26% after 6 h of shaking).^{11,14} Several techniques have been developed to bypass mechanical cutting with varying degrees of success.^{13,26,27,33,34} For example, intercalating graphite oxides with small molecules (*e.g.* CO_2 ²⁷ or tetrabutylammonium hydroxide²⁶) can generate electrostatic repulsive forces or internal pressure to exfoliate LGO sheets, producing flake sizes exceeding $330\text{ }\mu\text{m}^2$.²⁶ However, the efficiency and scalability of this process are currently unsatisfactory due to its long reaction time.

To understand the inherent limit imposed by the oxidation process on the size of the exfoliated graphene flakes, it is instructive to examine the mechanism of graphite oxidation. As shown in Fig. 2c, the oxidation of graphite takes place along two channels simultaneously: (1) the cross-planar oxidation which propagates along the *c*-axis direction and (2) the in-plane oxidation coming from the edge-to-center penetration of the oxidizer.¹⁴ The former follows the crack of the upper layer and facilitates the lateral penetration of the oxidizer solution between the layers, ultimately causing the deeper layers to crack in due course as a result of stress build-up.³² According to a study on the oxidation rate of highly ordered pyrolytic graphite (HOPG), the in-plane oxidation (v_p) rate is ~ 10 times larger than the rate of crack propagation (v_c , Fig. 2c).¹⁴ However, for thin graphite flakes with an aspect ratio of >10 , cross-planar cracking becomes the limiting factor in the lateral size of the graphene layers. We can see that it is difficult to achieve both high efficiency exfoliation and large sized GO sheets because the kinetic parameters (*e.g.* the concentration of the oxidizer, time, and reaction temperature) exert similar influences on both v_p and v_c .

A thermodynamic model has been used to analyze the cross-planar cracks, where the elastic strain energy (ΔE_s) released after cracking is considered as the sum of the crack formation energy (E_{crack}) and the work done for enlarging the interlayer spacing ($E_{\text{interlayer}}$).¹⁴ Since ΔE_s and $\Delta E_{\text{interlayer}}$ are based on thermodynamic parameters and E_{crack} is expressed as the product of bond energy and the average numbers of cracked

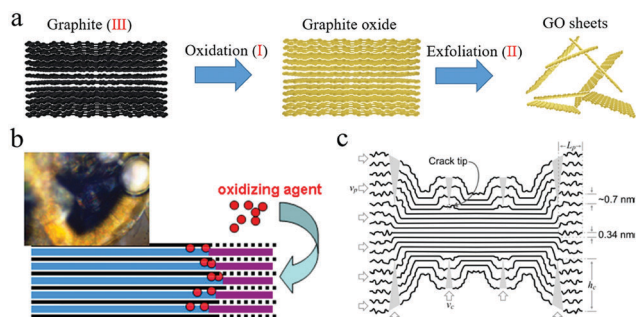


Fig. 2 (a) Schematic illustration of the graphite oxidation to exfoliation process. (b) Mechanism of diffusion-driven oxidation and the corresponding intermediate product. Adapted with permission from ref. 18. Copyright 2014 American Physical Society. (c) Crack propagation that resulted from cross-planar and edge-to-center oxidation. Adapted with permission from ref. 14. Copyright 2011 American Physical Society.

C–C bonds,¹⁴ the resultant crack-density is independent of the kinetic parameters. Note that E_s is much higher than $\Delta E_{\text{interlayer}}$,^{14,35,36} thus an efficient solution for decreasing the crack-density is to enlarge the interlayer spacing of graphite, which will weaken the elastic strain energy E_s . In fact, enlarging the interlayer spacing facilitates the penetration of the oxidizer and thus increases the rate of in-plane oxidation.

Improved efficiencies in exfoliating large GO nanosheets have been obtained by using thermally or microwave expanded graphite (TEG or MEG) as the starting material for chemical exfoliation.^{15,24,29} TEG and MEG show the signature “worm-like” appearance, which is created by interlayer gas-releasing reaction of the graphite intercalation compound (GIC), and consist of interconnected multilayer graphene sheets (45–68 of bonded graphene layers per unit).³⁷ Through the thermal expansion of the GIC and subsequent oxidation, LGO sheets with a mean size of 33 μm have been obtained.³⁸ However, these improvements are still far from ideal due to the low yield of LGO and the time-consuming process for size-fractionation. In fact, microstructural studies revealed that, notwithstanding the hundred fold volume expansion, TEM and MEG have accessible specific surface areas (SSAs) which are one order of magnitude lower compared to the same mass of free-standing monolayer graphene sheets.³⁹

Recently, Hongbin Lu and team proposed a scalable method for preparing high-quality graphene *via* chemically expanded graphite (CEG).^{40,41} CEG possesses open, porous microscopic structures with a high specific surface area ($> 840 \text{ m}^2 \text{ g}^{-1}$) that is nearly one order of magnitude larger than that of thermally expanded graphite (TEG), and close to the theoretical value of three-layered graphene sheets.⁴⁰ Different from TEG and MEG, which are prepared from rapid decomposition-reaction of the interlayer molecules, CEG is prepared through gentle, gas-releasing oxidation–reduction⁴⁰ or catalytic⁴² reaction between the intercalated molecules in the GIC and surrounding solution. The mild reaction facilitates the infiltration of interconnected liquid bodies within the interlayers and prevents the restacking of graphene layers.⁴³ For example, when CrO_3 -intercalated

graphite is immersed in H_2O_2 solution, the gas-releasing reactions within the interlayers produce CEG with ~ 1000 -fold volume expansion.⁴⁰ Kinetic modeling reveals that the microstructure of CEG greatly promotes the diffusion of solvent/solute molecules into graphite interlayer galleries.¹¹ In the oxidation step, the expanded interlayer spacing accelerates oxidizer diffusion and thus promotes CEG oxidation at a low temperature of 35 $^\circ\text{C}$ (Fig. 3a). Due to the expanded interlayer distance, the amount of the oxidizer needed is also reduced (2 wt equiv. relative to graphite), thus minimizing chemical cutting. In addition, mechanical stirring can also be avoided. GO derived from the chemically expanded graphite oxide (CEGO) prepared in this way retains its initial form without cracks along the in-plane direction. The accordion-like structure of CEGO dramatically simplifies GO-purification through sieve-filtration or standing, obviating the use of centrifugation or dialysis (Fig. 3b). Since the interlayer van der Waals interactions in CEGO are weakened by chemical expansion and oxidation, CEGO particles can be completely exfoliated in water by gentle mechanical agitation (5 min of stirring or 10 s of hand-shaking). Eventually, without size-fractionation, LGO sheets with a mean size of 83 μm can be obtained with $\sim 100\%$ yield (Fig. 3c). Besides weakened interlayer interactions, the surface wettability of CEG can be tuned to achieve the desired graphene exfoliation, dispersion, and performance optimization. For example, interlayer polymerization in CEG allows it to be spontaneously exfoliated into single- and few-layer graphene in poly(methyl methacrylate) (PMMA), opening an important route for the dispersion of LGO in polymers.⁴⁰

3. Unique properties and advanced applications

The performance of GO-based macrostructures in electronic, thermal and mechanical applications is highly dependent on the size of the GO sheets used in making these structures.^{5,6,11,44–47}

Multilayer-stacked graphene films derived separately from LGO and SGO (Fig. 4a and b) show markedly different properties,

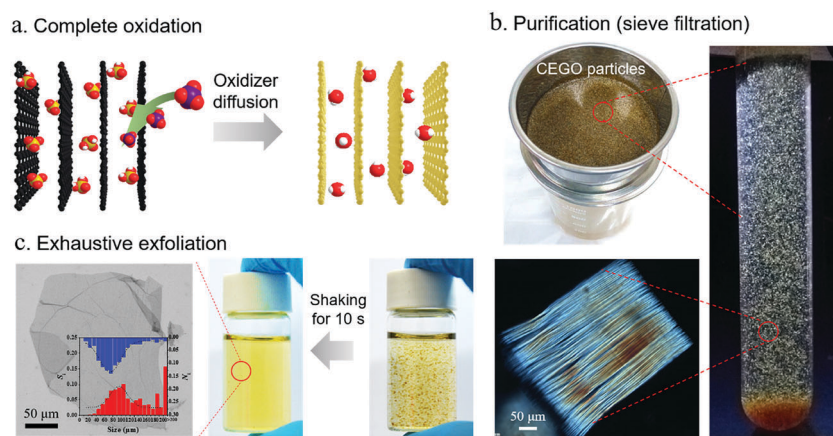


Fig. 3 (a–c) Fabrication processes of LGO by using CEG as the starting material. Reproduced with permission from ref. 11. Copyright 2017 American Chemical Society.

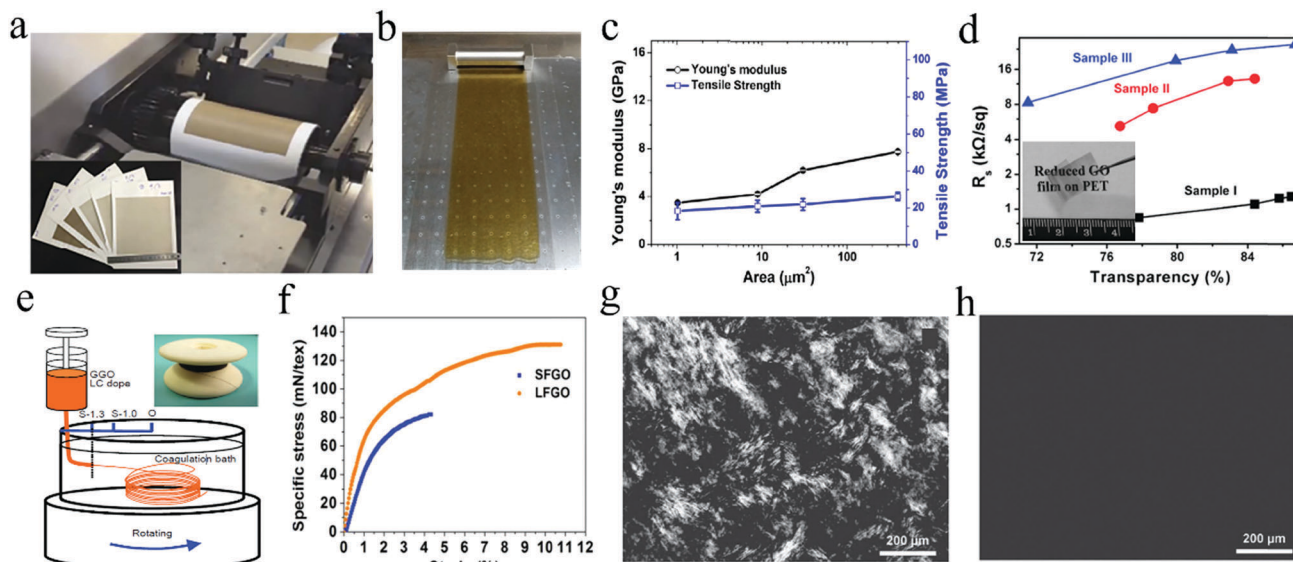


Fig. 4 (a and b) Gravure printing (a) and blade casting (b) to prepare large-area GO films. Panel a adapted with permission from ref. 44. Copyright 2016 Macmillan Publishers Ltd. Panel b adapted with permission from ref. 11. Copyright 2017 American Chemical Society. (c) Mechanical performance comparisons of LGO and SGO films. Adapted with permission from ref. 6. Copyright 2012 American Chemical Society. (d) Electrical conductivity comparison of LGO and SGO films after reduction. Adapted with permission from ref. 5. Copyright 2010 American Chemical Society. (e) Schematic fabrication of GO fibers. Adapted with permission from ref. 45. Copyright 2013 Wiley-VCH Verlag GmbH & Co. KGaA. (f) Specific stress–strain curves of LGO and SGO fibers. Adapted with permission from ref. 46. Copyright 2013 Wiley-VCH Verlag GmbH & Co. KGaA. (g and h) Size-dependent liquid crystalline behavior for well-ordered nematic LGO dispersion (g) and homogeneous isotropic SGO dispersion (h) at 1.5 mg ml^{-1} of concentration. Adapted with permission from ref. 9. Copyright 2015 Wiley-VCH Verlag GmbH & Co. KGaA.

and it is clear that the superiority of LGO-derived graphene films stems from the larger lateral size of the GO flakes. The lower density of inter-sheet junctions in LGO induces stronger mechanical performance, higher electrical/thermal conductivity and stronger electromagnetic interference shielding performance.^{6,11,13,48–51} For example, compared to SGO papers, LGO papers exhibit 320% improvement in Young's modulus and 280% improvement in tensile strength ($1.1 \mu\text{m}^2$ for SGO and $272 \mu\text{m}^2$ for LGO in mean area, Fig. 4c).⁶ After reduction, the electrical and thermal conductivities increase by 160% and 154%, respectively ($1 \mu\text{m}^2$ for SGO and $23 \mu\text{m}^2$ for LGO in mean area).¹³ These effects are especially pronounced in graphene-based transparent conducting films (Fig. 4d).⁵ One effect that must be considered is the positive role of epoxy oxygen groups in dissipating strain during ring opening reactions; in principle, this can have a bigger role in SGO due to its higher population of oxygen than LGO;^{52–54} however, evidence shows that size-effects still have a major influence on the mechanical performances of GO-based films and composites.^{5,6,9}

Similar results were also observed for LGO fibers, which exhibit significant improvements in specific stress and specific modulus (Fig. 4e).^{9,46,55} In addition, the knot efficiency, which represents the fiber strength when it is knotted or wound, reaches 100% for LGO fibers because of the lower bending modulus of LGO sheets than that of SGO sheets (Fig. 4f).⁴⁷ LGO dispersion tends to form a well-ordered nematic phase, while SGO dispersion remains a homogeneous isotropic phase at the same concentration (Fig. 4g and h).^{9,10,45,55} After extrusion or coating, LGO fibers/films possess a denser and more uniform

microstructure than SGO counterparts. Due to their larger area, LGO sheets also encapsulate silver nanowire networks more effectively than SGO sheets, leading to better performance in a transparent film heater.⁵⁶

Similar to the liquid crystalline phase, size also affects the rheological behavior of GO dispersions, including their viscosity, storage/loss modulus and critical gel concentration.^{11,12} For the LGO sheets described in Fig. 5a, typical physical gelation occurred at a very low concentration of 5 mg ml^{-1} . According to rheological studies, the storage and loss moduli of this LGO dispersion are approximately two orders of magnitude higher than those of SGO dispersion (Fig. 5b).^{10,11} This affords wide processing windows for various industrial fabrication techniques, including electrospray, spray coating, ink-jet printing, extrusion printing and dry-spinning (Fig. 5c).^{12,58} Under an applied electric field, LGO displays more sensitive rotational motion than SGO because of its higher polarizability; it induces the ordering of the surrounding small particles, giving an electro-optical switching performance.⁵⁹

In addition, when made into a monolithic porous material, LGO-based material performs better than SGO in electrical conductivity, mechanical strength and ion-absorption (Fig. 5d).^{57,60,61} For electrochemical applications, increasing the lateral size is beneficial to the electrical conductivity and stability of graphene-based anodes, which contributes to the improved cycle stability of lithium-/aluminum-ion batteries.^{62,63} Further evidence comes from the fact that LGO-based networks perform better in lithium-sulfur batteries than the SGO counterpart.⁶⁴ For biological applications, although SGO is generally favored for antimicrobial activity⁶⁵

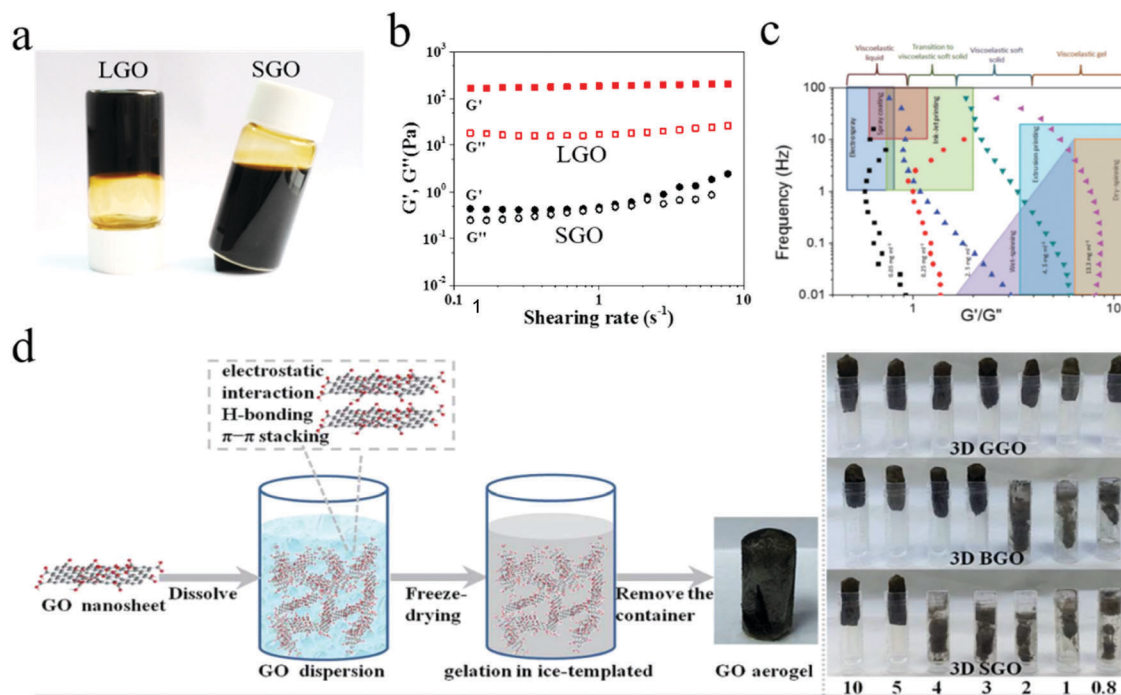


Fig. 5 (a and b) Significantly different gelation behaviors (a) and moduli (b) of LGO and SGO dispersions at 5 mg ml^{-1} of concentration. Reproduction with permission from ref. 11. Copyright 2017 American Chemical Society. (c) The correlation between rheological properties and approximate processing regimes for various applications. Adapted with permission from ref. 12. Copyright 2014 The Royal Society of Chemistry. (d) Schematic illustration of the size-dependent self-assembly of three-dimensional graphene-based macrostructures. Adapted with permission from ref. 57. Copyright 2016 The Royal Society of Chemistry.

and drug-delivery,⁶⁶ LGO exhibits a stronger positive influence on cell viability,⁶⁷ it can activate macrophages⁶⁸ and show reduced phagocytosis by cells.

4. Traditional reduction method

The functionality of LGO in applications can be dramatically improved by removing the oxygen to reduced GO. Reduction of GO is necessary to form reduced graphene oxide (rGO) in large quantities.^{69–73} Since the purpose of reduction is mainly to restore the high electrical conductivity of graphene, the latter parameter can be used as direct evidence to judge the effectiveness of the reduction methods. In general, high temperature thermal annealing or chemical reduction is used to remove oxygen functional groups on the GO surface. A common method is chemical reduction using hydrazine monohydrate.^{74,75} During the hydrazine reduction of GO sheets, ring-opening of epoxy groups occurs to form hydrazine alcohols, and the initial derivative produced by the epoxide opening reacts further to form an aziridine moiety, which then undergoes thermal elimination of di-imide to form a double bond.⁷⁶ An electrically conductive black precipitate with a C/O elemental ratio of ~ 10 can be obtained.^{74,77} The highest conductivity of rGO films produced by hydrazine reduction is 99.6 S cm^{-1} , with a C/O elemental ratio of around 12.5.⁷⁸ One reason for the poor electrical conductivity is the partial deoxygenation and recovery of the conjugated bonds,

hydrazine reduction can reduce only epoxy groups, and has no effects on the hydroxyl, carbonyl and carboxyl groups of GO.⁷⁹

Park *et al.* used ^{13}C and ^{15}N solid-state nuclear magnetic resonance spectroscopy and X-ray photoelectron spectroscopy to study the chemical structure of hydrazine-treated rGO. Their study suggests that the hydrazine treatment of GO causes insertion of an aromatic N_2 moiety into a five-membered ring at the edges of the sheets⁸⁰ (Fig. 6a and b). Several authors have reported the thermal method of rGO paper/fibers through thermal reduction, resulting in products with high conductivity.^{73,81,82} Xin *et al.* reported the electrical conductivity of free standing graphene paper to be $\sim 1.57 \times 10^5 \text{ S m}^{-1}$ produced *via* thermal annealing at $2200 \text{ }^\circ\text{C}$.⁸³ Shen *et al.* achieved an electrical conductivity of 1000 S m^{-1} through high temperature reduction of rGO at $2000 \text{ }^\circ\text{C}$.⁸⁴ Reduction at elevated temperatures removes most of the oxygen functional groups and restores the sp^2 conjugation to a large extent. However, this may come with collateral damage, since CO and CO_2 gas are formed, which indicates the removal of carbon atoms and the creation of defects in the basal plane. High temperature annealing also increases the cost of mass production. In addition, oxygen functional groups form highly stable ether and carbonyl groups that are difficult to remove so that rGO contains a residual oxygen concentration of 15 to 25 at% (Fig. 6c and d).⁸⁵

Hydroiodic acid (HI) has also been used to reduce GO.^{86,87} This study showed similar reduction results in that the C/O ratio of rGO is around 15, and the conductivity of the rGO films is around 300 S cm^{-1} , which is much better than those

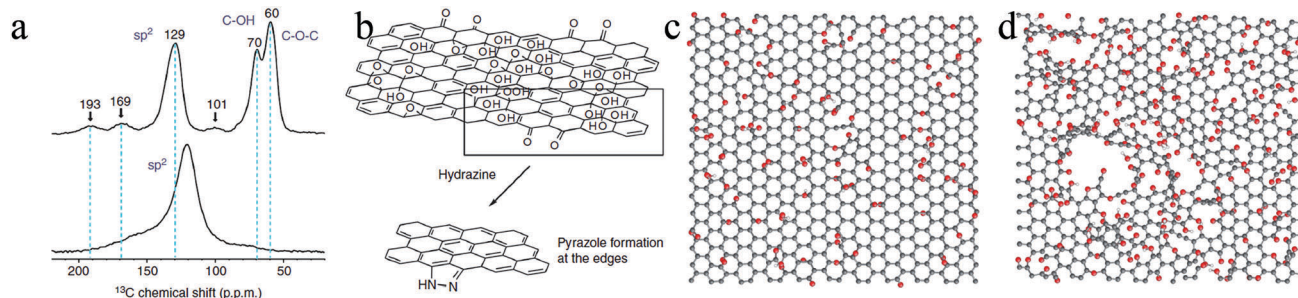


Fig. 6 Chemical structures of labelled samples before and after hydrazine treatment. (a) ^{13}C MASS SSNMR spectra of (top) ^{13}C -labelled GO and (bottom) ^{13}C - and ^{15}N -labelled RGO. (b) A schematic illustrating pyrazole formation at the edges of the platelets during the hydrazine treatment of graphene oxide ($-\text{COOH}$ groups at the platelet edges have been omitted for clarity). (c) Morphology of rGO and the structure of defects formed during thermal annealing. Morphology of rGO sheets with an initial oxygen concentration of (c) 20% and (d) 33% in the form of hydroxyl and epoxy groups at a ratio of 3/2 after annealing at 1500 K.

obtained *via* hydrazine reduction methods (Fig. 7a–d). The GO film reduced by HI has good flexibility and even improved tensile strength, while the hydrazine vapor-reduced GO film becomes too rigid to be rolled and the film thickness expanded more than 10 times (Fig. 7b and c). This is attributed to the fact that during hydrazine treatment of the GO film, significant bubbling and expansion occur, which lead to fragmentation and mechanical instability. In contrast, the film reduced by HI shows a reduction in GO film thickness due to reduction. This densification of the reduced GO film also improves its mechanical properties. The appearance of the 2D peak in the Raman spectrum indicates the partial restoration of sp^2 carbon in the rGO film (Fig. 7e). These results show that HI not only has a better reducing effect than hydrazine, but is also suitable for the reduction of GO films.

In contrast to chemical reduction methods, photo- and electrochemical reduction avoid the use of toxic chemicals and solvents that can create hazardous waste.^{88–90} Guo *et al.* reported a simple approach for achieving good quality rGO using electrochemical reduction of GO at a cathodic potential of 1.5 V. The high negative potential was found to overcome the

energy barrier for the removal of oxygen functional groups, giving rise to an electrical conductivity of 350 S cm^{-1} .⁸⁸ Photo-reduction works by generating hydrated electrons from water under ultraviolet (UV) irradiation, and these can be powerful reductants for reducing GO in aqueous solutions.⁹⁰ Gengler *et al.* investigated the mechanism of photoreduction of GO in solution using femtosecond laser pulses. They found that an ultrafast photoinduced chain reaction was initiated by the femtosecond ultraviolet pulse, leading to the photoionization of solvent and liberation of solvated electrons that trigger the reduction.⁹¹ In terms of compatibility with microelectronic processing, the photothermal reduction of GO films using lasers allows conducting lines made of rGO to be written in GO. The ability to reduce GO films by laser annealing has been exploited to create optical modulation patterns consisting of alternating rGO and GO strips. Taking advantage of the difference in refractive index and optical transmission between rGO and GO, the optical modulation pattern that is created can afford a lens focusing effect and wavefront shaping, thus making rGO/GO a promising platform for next-generation ultrathin, light-weight and flexible photonic and optoelectronic

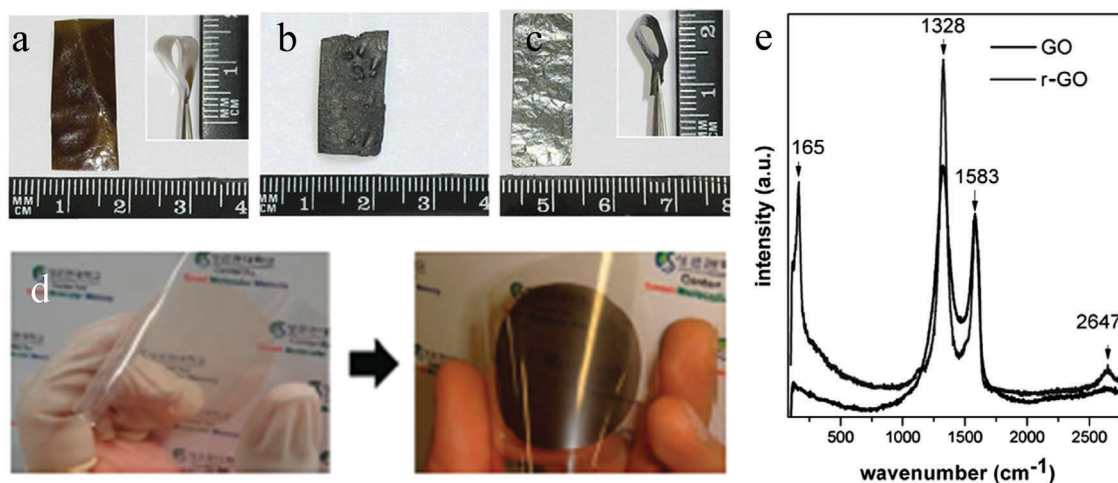


Fig. 7 Optical photographs of GO films (a) before (b and c) after chemical reduction by different agents: (b) hydrazine vapor and (c) HI. (d) Flexible GO (left) and rGO thin films reduced by HI on a PET substrate. (e) Raman spectrum of HI treated rGO.

applications. Using the laser writing approach on GO, Jia *et al.* has demonstrated far-field 3D subwavelength focusing ($\lambda^3/5$) with an absolute focusing efficiency $>32\%$ over a broad wavelength range from 400 to 1500 nm.⁹²

New approach for reduction

Functional groups are relatively easy to remove, whereas defects, whether formed during oxidation or reduction, are difficult to heal by reduction. Thus, the concentration of defects in the basal plane of rGO is the key to determine whether GO sheets can be well reduced. Chen *et al.* achieved high conductivity in rGO films through an electrical current-induced annealing process at 2750 K for less than 1 min of annealing time⁹³ (Fig. 8a). Different from traditional thermal treatment in a furnace, Joule heating can generate ultrahigh temperature at junction points where the higher electrical resistance is located. The self-healing thermal reduction may have the possibility of forming cross-links between adjacent rGO at defects, which helps in constructing highly dense rGO films, leading to a high electrical conductivity of up to 3112 S cm^{-1} (Fig. 7d and e). The decreased $I_{\text{D}}/I_{\text{G}}$ ratio dramatically indicates that the Joule-heated rGO film can become highly crystallized (Fig. 8b and c). In addition, a sharp 2D peak (2690 cm^{-1}) can be observed after Joule heating, with an $I_{2\text{D}}/I_{\text{G}}$ ratio of 0.93, confirming the highly crystalline structure of the rGO film after the Joule heating process. Recently, Xin *et al.* reported a way to make coiled graphene fibers with high mechanical strength and thermal conductivity by intercalating small fragments of rGO into gaps formed by LGO, and subjecting them to a high temperature anneal of

$2850 \text{ }^\circ\text{C}$.⁹⁴ As shown in Fig. 8, LGO sheets form a highly aligned backbone, while SGO sheets filled the space and voids in the fiber. The high temperature annealing creates submicrometer crystallite domain size in the graphene fibers and makes effective interconnection at junctions, achieving an enhanced thermal conductivity of up to $1290 \text{ W m}^{-1} \text{ K}^{-1}$ and a tensile strength of 1080 MPa.

Microwave reduction technology, which is industrially scalable, has great potential for the reduction of GO at a lower energy cost compared to high temperature annealing, but the efficiency of reduction is low. Recently, Voiry *et al.* used a conventional microwave setup to reduce GO with 1- to 2-pulses of microwaves (Fig. 8f).⁹⁵ They slightly annealed the GO prior to exposure to microwaves to improve its conductivity so it could absorb microwaves. Using this method, the D peak intensity of microwave-reduced graphene oxide (MW-rGO) is dramatically reduced, whereas the restoration of the 2D band shows that the structure of sp^2 carbon for MW-rGO is largely restored (Fig. 8h and i), such that the $I_{2\text{D}}/I_{\text{G}}$ ratio is close to or higher than 1. Significantly, the evolution of the D and 2D peaks differs from thermally annealed rGO samples even after annealing at temperatures as high as $1000 \text{ }^\circ\text{C}$.

Chemical reduction does not only result in the removal of oxygen groups, it can be used for hydrogenation of unsaturated bonds. For example, in the Birch reduction, solvated electrons in sodium-ammonia solution facilitate the de-oxygenation of graphene oxide and the restoration of the sp^2 network.⁹⁶ It is known that unconjugated cyclohexadienes can be reduced by a 1,4-reduction in the Birch reduction; thus it can be expected

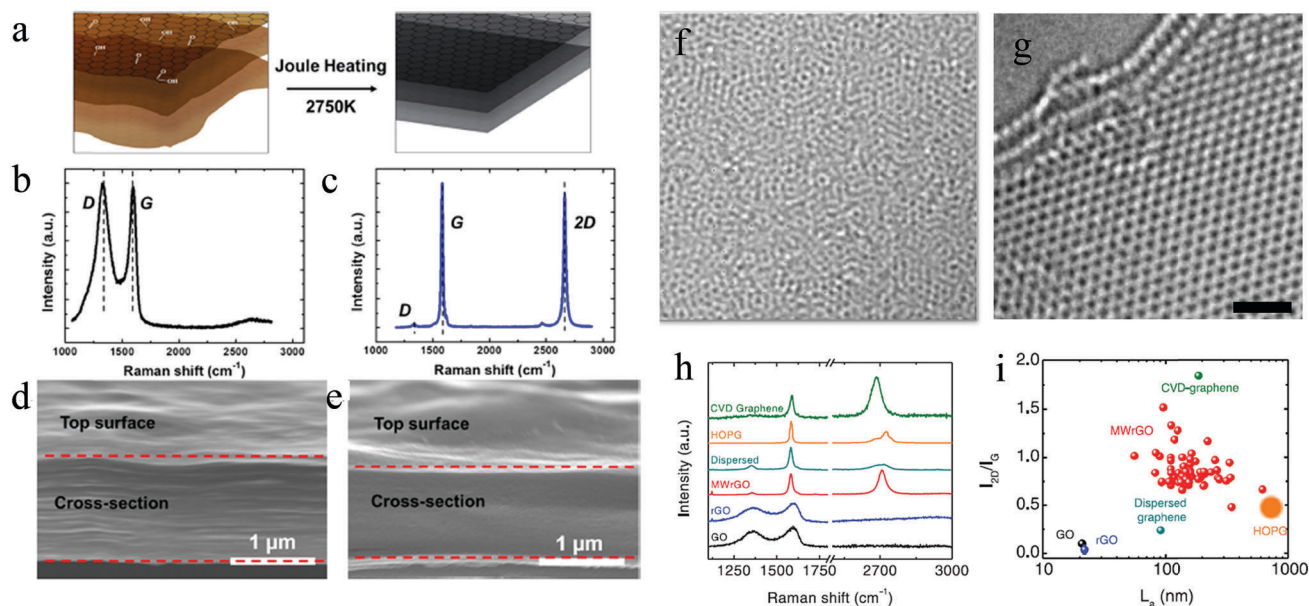


Fig. 8 (a) Joule heating at 2750 K for 1 min in a vacuum can effectively reduce the rGO. Raman spectrum comparison of a rGO film annealed in a furnace at (b) 773 K and the same film after (c) the 2750 K annealing for 1 min. The low D/G ratio and the high 2D peak indicate highly crystalline rGO nanosheets after reduction. (d and e) Cross-section SEM images of the rGO film before and after the Joule heating. The Joule heating effectively densifies the rGO films, which significantly increases the coupling in charge transport. (f) High-resolution TEM image of disordered GO and (g) MW-rGO showing a highly ordered structure. Scale bars, 1 nm. (h) Raman spectra of MW-rGO and other graphene-based samples. (i) Evolution of the $I_{2\text{D}}/I_{\text{G}}$ ratio versus the crystal size (L_{c}) for MW-rGO, GO, rGO, highly ordered pyrolytic graphite (HOPG), dispersed graphene, and graphene.

that the aromatic framework in graphene can be hydrogenated if protons are present. Pumera *et al.* show that the choice of alkali metals and alcohols/water as quenching agents affects the hydrogenation yield. A systematic study of electron (Li, Na, K, Cs) and proton sources (*t*BuOH, *i*PrOH, MeOH, H₂O) has been performed to identify optimal conditions for hydrogenation of graphene oxide.⁹⁷

5. Conclusion

This review examines recent advances in the synthesis and reduction of GO. The lateral size of GO sheets exerts a key influence on the properties of GO-derived layered architectures and 3D networks since properties such as thermal, electrical and mechanical strengths are related to in-plane long-range order. Although SGO flakes are commonly researched and manufactured commercially, LGO sheets are highly desirable for both research and industrial applications. Changes in manufacturing processes are needed for producing LGO. These include using chemically expanded graphite instead of graphite oxide as the starting material, in combination with a low energy agitation process. To use LGO as heat sinks or electrical conductive coatings, an efficient reduction process which can remove completely the oxygen functional groups and recover the sp² conjugation is needed. Recent work shows that rapid Joule or microwave heating leads to an almost complete removal of oxygen functional groups and repairs the highly ordered conjugated sp² structure. Due to the lower content of oxygen groups on LGO, it should be readily reduced to graphene with a low concentration of defects, and will offer substantial performance enhancement to macroscopic components fabricated from it.

Conflicts of interest

There are no conflicts to declare.

Acknowledgements

K. P. Loh thanks the National Research Foundation, Singapore, for an NRF Investigator Award: "Graphene oxide a new class of catalytic, ionic and molecular sieving materials, award number: NRF-NRF12015-01".

References

- G. Xin, T. Yao, H. Sun, S. M. Scott, D. Shao, G. Wang and J. Lian, Highly thermally conductive and mechanically strong graphene fibers, *Science*, 2015, **349**, 1083–1087.
- Y. Zhu, S. Murali, M. D. Stoller, K. J. Ganesh, W. Cai, P. J. Ferreira, A. Pirkle, R. M. Wallace, K. A. Cychoz, M. Thommes, D. Su, E. A. Stach and R. S. Ruoff, Carbon-based supercapacitors produced by activation of graphene, *Science*, 2011, **332**, 1537–1541.
- T. Shen, S.-H. Hong and J.-K. Song, Electro-optical switching of graphene oxide liquid crystals with an extremely large Kerr coefficient, *Nat. Mater.*, 2014, **13**, 394–399.
- J. Abraham, K. S. Vasu, P. Carbone, A. K. Geim and R. R. Nair, Tunable sieving of ions using graphene oxide membranes, *Nat. Nanotechnol.*, 2017, **12**, 546–550.
- J. Zhao, S. Pei, W. Ren, L. Gao and H. Cheng, Efficient preparation of large-area graphene oxide sheets for transparent conductive films, *ACS Nano*, 2010, **4**, 5245–5252.
- X. Lin, X. Shen, Q. Zheng, N. Yousefi, L. Ye, Y. Mai and J. Kim, Fabrication of highly-aligned, conductive, and strong graphene papers using ultralarge graphene oxide sheets, *ACS Nano*, 2012, **6**, 10708–10719.
- X. Liu, G. Zhang and Y.-W. Zhang, Thermal conduction across graphene cross-linkers, *J. Phys. Chem. C*, 2014, **118**, 12541–12547.
- B. Mi, Graphene oxide membranes for ionic and molecular sieving, *Science*, 2014, **343**, 740–742.
- M. Z. Seyedin, J. M. Razal, P. C. Innis, R. Jalili and G. G. Wallace, Achieving outstanding mechanical performance in reinforced elastomeric composite fibers using large sheets of graphene oxide, *Adv. Funct. Mater.*, 2015, **25**, 94–104.
- R. Jalili, S. H. Aboutalebi, D. Esrafilzadeh, K. Konstantinov, J. M. Razal, S. E. Moulton and G. G. Wallace, Formation and processability of liquid crystalline dispersions of graphene oxide, *Mater. Horiz.*, 2014, **1**, 87–91.
- L. Dong, Z. X. Chen, S. Lin, K. Wang, C. Ma and H. B. Lu, Reactivity-controlled preparation of ultralarge graphene oxide by chemical expansion of graphite, *Chem. Mater.*, 2017, **29**, 564–572.
- S. Naficy, R. Jalili, S. H. Aboutalebi, R. A. Gorkin III, K. Konstantinov, P. C. Innis, G. M. Spinks, P. Poulin and G. G. Wallace, Graphene oxide dispersions: tuning rheology to enable fabrication, *Mater. Horiz.*, 2014, **1**, 326–331.
- P. Kumar, F. Shahzad, S. Yu, S. M. Hong, Y.-H. Kim and C. M. Koo, Large-area reduced graphene oxide thin film with excellent thermal conductivity and electromagnetic interference shielding effectiveness, *Carbon*, 2015, **94**, 494–500.
- S. Pan and I. A. Aksay, Factors controlling the size of graphene oxide sheets produced via the graphite oxide route, *ACS Nano*, 2011, **5**, 4073–4083.
- J. Jia, C. Kan, X. Lin, X. Shen and J. Kim, Effects of processing and material parameters on synthesis of monolayer ultralarge graphene oxide sheets, *Carbon*, 2014, **77**, 244–254.
- J. Li, K. N. Kudin, M. J. McAllister, R. K. Prud'homme, I. A. Aksay and R. Car, Oxygen-driven unzipping of graphitic materials, *Phys. Rev. Lett.*, 2006, **96**, 176101.
- R. K. Singh, R. Kumar and D. P. Singh, Graphene oxide: strategies for synthesis, reduction and frontier applications, *RSC Adv.*, 2016, **6**, 64993–65011.
- A. M. Dimiev and J. M. Tour, Mechanism of graphene oxide formation, *ACS Nano*, 2014, **8**, 3060–3068.
- W. S. Hummers and R. E. Offeman, Preparation of graphitic oxide, *J. Am. Chem. Soc.*, 1958, **80**, 1339.

- 20 L. Peng, Z. Xu, Z. Liu, Y. Y. Wei, H. Y. Sun, Z. Li, X. L. Zhao and C. Gao, An iron-based green approach to 1-h production of single-layer graphene oxide, *Nat. Commun.*, 2015, **6**, 5716.
- 21 D. C. Marcano, D. V. Kosynkin, J. M. Berlin, A. Sinitskii, Z. Sun, A. Slesarev, L. B. Alemany, W. Lu and J. M. Tour, Improved synthesis of graphene oxide, *ACS Nano*, 2010, **4**, 4806–4814.
- 22 C. K. Chua, Z. Sofer and M. Pumera, Graphite oxides: effects of permanganate and chlorate oxidizers on the oxygen composition, *Chem. – Eur. J.*, 2012, **18**, 13453–13459.
- 23 C.-Y. Su, Y. Xu, W. Zhang, J. Zhao, X. Tang, C.-H. Tsai and L.-J. Li, Electrical and spectroscopic characterizations of ultra-large reduced graphene oxide monolayers, *Chem. Mater.*, 2009, **21**, 5674–5680.
- 24 Z. Luo, Y. Lu, L. A. Somers and A. T. C. Johnson, High yield preparation of macroscopic graphene oxide membranes, *J. Am. Chem. Soc.*, 2009, **131**, 898–899.
- 25 S. Wang, P. K. Ang, Z. Q. Wang, A. L. L. Tang, J. T. L. Thong and K. P. Loh, High mobility, printable, and solution-processed graphene electronics, *Nano Lett.*, 2010, **10**, 92–98.
- 26 P. K. Ang, S. Wang, Q. Bao, J. T. L. Thong and K. P. Loh, High-throughput synthesis of graphene by intercalation-exfoliation of graphite oxide and study of ionic screening in graphene transistor, *ACS Nano*, 2009, **3**, 3587–3594.
- 27 D. W. Kim, D. Kim, B. H. Min, H. Lee and H. Jung, Sonication-free dispersion of large-area graphene oxide sheets using internal pressure from release of intercalated carbon dioxide, *Carbon*, 2015, **88**, 126–132.
- 28 X. Zhou and Z. Liu, A scalable, solution-phase processing route to graphene oxide and graphene ultralarge sheets, *Chem. Commun.*, 2010, **46**, 2611–2613.
- 29 Q. Zheng, W. H. Ip, X. Lin, N. Yousefi, K. K. Yeung, Z. Li and J. Kim, Transparent conductive films consisting of ultra-large graphene sheets produced by Langmuir-Blodgett assembly, *ACS Nano*, 2011, **5**, 6039–6051.
- 30 U. Hofmann and E. König, Untersuchungen über graphitoxid, *Z. Anorg. Allg. Chem.*, 1937, **234**, 311–336.
- 31 L. Staudenmaier, Verfahren zur darstellung der graphitsäure, *Ber. Dtsch. Chem. Ges.*, 1898, **31**, 1481–1487.
- 32 P. M. Ajayan and B. I. Yakobson, Oxygen breaks into carbon world, *Nature*, 2006, **441**, 818–819.
- 33 N. Kovtyukhova, P. J. Ollivier, B. R. Martin, T. E. Mallouk, S. A. Chizhik, E. V. Buzaneva and A. D. Gorchinskiy, Layer-by-layer assembly of ultrathin composite films from micro-sized graphite oxide sheets and polycations, *Chem. Mater.*, 1999, **11**, 771–778.
- 34 I. Ogino, Y. Yokoyama, S. Iwamura and S. R. Mukai, Exfoliation of graphite oxide in water without sonication: bridging length scales from nanosheets to macroscopic materials, *Chem. Mater.*, 2014, **26**, 3334–3339.
- 35 H. C. Schniepp, K. N. Kudin, J.-L. Li, R. K. Prud'homme, R. Car, D. A. Saville and I. A. Aksay, Bending properties of single functionalized graphene sheets probed by atomic force microscopy, *ACS Nano*, 2008, **2**, 2577–2584.
- 36 M. Lotya, Y. Hernandez, P. J. King, R. J. Smith, V. Nicolosi, L. S. Karlsson, F. M. Blighe, S. De, Z. Wang, I. T. McGovern, G. S. Duesberg and J. N. Coleman, Liquid phase exfoliation of graphene by exfoliation of graphite in surfactant/water solutions, *J. Am. Chem. Soc.*, 2009, **131**, 3611–3620.
- 37 A. Celzard, J. F. Maréché and G. Furdin, Modelling of exfoliated graphite, *Prog. Mater. Sci.*, 2005, **50**, 93–179.
- 38 S. H. Aboutalebi, M. M. Gudarzi, Q. B. Zheng and J. Kim, Spontaneous formation of liquid crystals in ultralarge graphene oxide dispersions, *Adv. Funct. Mater.*, 2011, **21**, 2978–2988.
- 39 A. Celzard, J. F. Maréché and G. Furdin, Surface area of compressed expanded graphite, *Carbon*, 2002, **40**, 2713–2718.
- 40 S. Lin, L. Dong, J. Zhang and H. Lu, Room-temperature intercalation and ~1000-fold chemical expansion for scalable preparation of high-quality graphene, *Chem. Mater.*, 2016, **28**, 2138–2146.
- 41 P. Wang, J. Zhang, L. Dong, C. Sun, X. Zhao, Y. Ruan and H. Lu, Interlayer polymerization in chemically expanded graphite for preparation of highly conductive, mechanically strong polymer composites, *Chem. Mater.*, 2017, **29**, 3412–3422.
- 42 X. M. Geng, Y. F. Guo, D. F. Li, W. W. Li, C. Zhu, X. F. Wei, M. L. Chen, S. Gao, S. Q. Qiu, Y. P. Gong, L. Q. Wu, M. S. Long, M. T. Sun, G. B. Pan and L. W. Liu, Interlayer catalytic exfoliation realizing scalable production of large-size pristine few-layer graphene, *Sci. Rep.*, 2013, **3**, 1134.
- 43 X. W. Yang, J. W. Zhu, L. Qiu and D. Li, Bioinspired effective prevention of restacking in multilayered graphene films: towards the next generation of high-performance supercapacitors, *Adv. Mater.*, 2011, **23**, 2833–2838.
- 44 D. A. Dikin, S. Stankovich, E. J. Zimney, R. D. Piner, G. H. B. Dommett, G. Evmenenko, S. T. Nguyen and R. S. Ruoff, Preparation and characterization of graphene oxide paper, *Nature*, 2007, **448**, 457–460.
- 45 A. Akbari, P. Sheath, S. T. Martin, D. B. Shinde, M. Shaibani, P. C. Banerjee, R. Tkacz, D. Bhattacharyya and M. Majumder, Large-area graphene-based nanofiltration membranes by shear alignment of discotic nematic liquid crystals of graphene oxide, *Nat. Commun.*, 2016, **7**, 10891.
- 46 Z. Xu, H. Sun, X. Zhao and C. Gao, Ultrastrong fibers assembled from giant graphene oxide sheets, *Adv. Mater.*, 2013, **25**, 188–193.
- 47 C. Xiang, C. C. Young, X. Wang, Z. Yan, C.-C. Hwang, G. Ceriotti, J. Lin, J. Kono, M. Pasquali and J. M. Tour, Large flake graphene oxide fibers with unconventional 100% knot efficiency and highly aligned small flake graphene oxide fibers, *Adv. Mater.*, 2013, **25**, 4592–4597.
- 48 H. Malekpour, K.-H. Chang, J.-C. Chen, C.-Y. Lu, D. L. Nika, K. S. Novoselov and A. A. Balandin, Thermal conductivity of graphene laminate, *Nano Lett.*, 2014, **14**, 5155–5161.
- 49 P. Kumar, S. Yu, F. Shahzad, S. M. Hong, Y.-H. Kim and C. M. Koo, Ultrahigh electrically and thermally conductive self-aligned graphene/polymer composites using large-area reduced graphene oxides, *Carbon*, 2016, **101**, 120–128.
- 50 J. Chen, Y. Li, L. Huang, N. Jia, C. Li and G. Shi, Size fractionation of graphene oxide sheets via filtration through track-etched membranes, *Adv. Mater.*, 2015, **27**, 3654–3660.
- 51 Y.-J. Wan, P.-L. Zhu, S.-H. Yu, R. Sun, C.-P. Wong and W.-H. Liao, Graphene paper for exceptional EMI shielding

- performance using large-sized graphene oxide sheets and doping strategy, *Carbon*, 2017, **122**, 74–81.
- 52 D. Liu, Q. Bian, Y. Li, Y. Wang, A. Xiang and H. Tian, Effect of oxidation degrees of graphene oxide on the structure and properties of poly(vinyl alcohol) composite films, *Compos. Sci. Technol.*, 2016, **129**, 146–152.
- 53 X. Wei, L. Mao, R. A. Soler-Crespo, J. T. Paci, J. Huang and H. D. Espinosa, Plasticity and ductility in graphene oxide through a mechanochemically induced damage tolerance mechanism, *Nat. Commun.*, 2015, **6**, 8029.
- 54 X. Sun, D. Luo, J. Liu and D. G. Evans, Monodisperse chemically modified graphene obtained by density gradient ultracentrifugal rate separation, *ACS Nano*, 2010, **4**, 3381–3389.
- 55 S. Seyedin, J. M. Razal, P. C. Innis, R. Jalili and G. G. Wallace, Compositional effects of large graphene oxide sheets on the spinnability and properties of polyurethane composite fibers, *Adv. Mater. Interfaces*, 2016, **3**, 1500672.
- 56 X. Zhang, X. Yan, J. Chen and J. Zhao, Large-size graphene microsheets as a protective layer for transparent conductive silver nanowire film heaters, *Carbon*, 2014, **69**, 437–443.
- 57 Y. Shen, X. Zhu and B. Chen, Size effects of graphene oxide nanosheets on the construction of three-dimensional graphene-based macrostructures as adsorbents, *J. Mater. Chem. A*, 2016, **4**, 12106–12118.
- 58 P. He and B. Derby, Inkjet printing ultra-large graphene oxide flakes, *2D Mater.*, 2017, **4**, 021021.
- 59 R. T. M. Ahmad, T.-Z. Shen, A. R. Masud, T. K. Ekanayaka, B. Lee and J.-K. Song, Guided electro-optical switching of small graphene oxide particles by larger ones in aqueous dispersion, *Langmuir*, 2016, **32**, 13458–13463.
- 60 Y.-D. Gao, Q.-Q. Kong, Z. Liu, X.-M. Li, C.-M. Chen and R. Cai, Graphene oxide aerogels constructed using large or small graphene oxide with different electrical, mechanical and adsorbent properties, *RSC Adv.*, 2016, **6**, 9851–9856.
- 61 K. E. Lee, J. J. Oh, T. Yun and S. O. Kim, Liquid crystallinity driven highly aligned large graphene oxide composites, *J. Solid State Chem.*, 2015, **224**, 115–119.
- 62 L. Zhang, L. Chen, H. Luo, X. Zhou and Z. Liu, Large-sized few-layer graphene enables an ultrafast and long-life aluminum-ion battery, *Adv. Energy Mater.*, 2017, 1700034.
- 63 S. Liu, G. Wang, H. Hou, X. Liu, J. Duan and Q. Liao, Binder-free combination of large area reduced graphene oxide nanosheets with Cu foil for lithium ion battery anode, *Diamond Relat. Mater.*, 2016, **68**, 102–108.
- 64 C.-Y. Fan, H.-H. Li, L.-L. Zhang, H.-Z. Sun, X.-L. Wu, H.-M. Xie and J.-P. Zhang, Fabrication of functionalized polysulfide reservoirs from large graphene sheets to improve the electrochemical performance of lithium-sulfur batteries, *Phys. Chem. Chem. Phys.*, 2015, **17**, 23481–23488.
- 65 F. Perreault, A. F. De Faria, S. Nejati and M. Elimelech, Antimicrobial properties of graphene oxide nanosheets: why size matters, *ACS Nano*, 2015, **9**, 7226–7236.
- 66 Z. Liu, J. T. Robinson, X. Sun and H. Dai, PEGylated nanographene oxide for delivery of water-insoluble cancer drugs, *J. Am. Chem. Soc.*, 2008, **130**, 10876–10877.
- 67 C. Wu, C. Wang, J. Zheng, C. Luo, Y. Li, S. Guo and J. Zhang, Vacuolization in cytoplasm and cell membrane permeability enhancement triggered by micrometer-sized graphene oxide, *ACS Nano*, 2015, **9**, 7913–7924.
- 68 J. Ma, R. Liu, X. Wang, Q. Liu, Y. Chen, R. P. Valle, Y. Y. Zuo, T. Xia and S. Liu, Crucial role of lateral size for graphene oxide in activating macrophages and stimulating pro-inflammatory responses in cells and animals, *ACS Nano*, 2015, **9**, 10498–10515.
- 69 K. P. Loh, Q. Bao, P. K. Ang and J. Yang, The chemistry of graphene, *J. Mater. Chem.*, 2010, **20**, 2277–2289.
- 70 W. Gao, L. B. Alemany, L. Ci and P. M. Ajayan, New insights into the structure and reduction of graphite oxide, *Nat. Chem.*, 2009, **1**, 403–408.
- 71 D. R. Dreyer, S. Park, C. W. Bielawski and R. S. Ruoff, The chemistry of graphene oxide, *Chem. Soc. Rev.*, 2009, **39**, 228–240.
- 72 S. Park and R. S. Ruoff, Chemical methods for the production of graphenes, *Nat. Nanotechnol.*, 2009, **4**, 217–224.
- 73 C. Kiang Chua and M. Pumera, Chemical reduction of graphene oxide: a synthetic chemistry viewpoint, *Chem. Soc. Rev.*, 2014, **43**, 291–312.
- 74 S. Stankovich, *et al.*, Synthesis of graphene-based nanosheets via chemical reduction of exfoliated graphite oxide, *Carbon*, 2007, **45**, 1558–1565.
- 75 V. C. Tung, M. J. Allen, Y. Yang and R. B. Kaner, High-throughput solution processing of large-scale graphene, *Nat. Nanotechnol.*, 2009, **4**, 25–29.
- 76 P. M. Lahti, Aziridinamine chemistry, I. – thermal decomposition of *cis* and *trans*-2,3-diphenylaziridinamine, *Tetrahedron Lett.*, 1983, **24**, 2339–2342.
- 77 S. Pei and H.-M. Cheng, The reduction of graphene oxide, *Carbon*, 2012, **50**, 3210–3228.
- 78 M. J. Fernández-Merino, *et al.*, Vitamin C Is an Ideal Substitute for Hydrazine in the Reduction of Graphene Oxide Suspensions, *J. Phys. Chem. C*, 2010, **114**, 6426–6432.
- 79 X. Gao, J. Jang and S. Nagase, Hydrazine and Thermal Reduction of Graphene Oxide: Reaction Mechanisms, Product Structures, and Reaction Design, *J. Phys. Chem. C*, 2010, **114**, 832–842.
- 80 S. Park, *et al.*, Chemical structures of hydrazine-treated graphene oxide and generation of aromatic nitrogen doping, *Nat. Commun.*, 2012, **3**, 638.
- 81 X. Li, *et al.*, Highly conducting graphene sheets and Langmuir-Blodgett films, *Nat. Nanotechnol.*, 2008, **3**, 538–542.
- 82 L. Song, *et al.*, Effect of high-temperature thermal treatment on the structure and adsorption properties of reduced graphene oxide, *Carbon*, 2013, **52**, 608–612.
- 83 G. Xin, *et al.*, Large-Area Freestanding Graphene Paper for Superior Thermal Management, *Adv. Mater.*, 2014, **26**, 4521–4526.
- 84 B. Shen, W. Zhai and W. Zheng, Ultrathin Flexible Graphene Film: An Excellent Thermal Conducting Material with Efficient EMI Shielding, *Adv. Funct. Mater.*, 2014, **24**, 4542–4548.
- 85 A. Bagri, *et al.*, Structural evolution during the reduction of chemically derived graphene oxide, *Nat. Chem.*, 2010, **2**, 581–587.

- 86 S. Pei, J. Zhao, J. Du, W. Ren and H.-M. Cheng, Direct reduction of graphene oxide films into highly conductive and flexible graphene films by hydrohalic acids, *Carbon*, 2010, **48**, 4466–4474.
- 87 I. K. Moon, J. Lee, R. S. Ruoff and H. Lee, Reduced graphene oxide by chemical graphitization, *Nat. Commun.*, 2010, **1**, 73.
- 88 H.-L. Guo, X.-F. Wang, Q.-Y. Qian, F.-B. Wang and X.-H. Xia, A Green Approach to the Synthesis of Graphene Nanosheets, *ACS Nano*, 2009, **3**, 2653–2659.
- 89 X. Feng, W. Chen and L. Yan, Electrochemical reduction of bulk graphene oxide, *RSC Adv.*, 2016, **6**, 80106.
- 90 Y. H. Ding, P. Zhang, Q. Zhao, H. M. Ren, Z. M. Yang and Y. Jiang, A green approach to the synthesis of reduced graphene oxide nanosheets under UV irradiation, *Nanotechnology*, 2011, **22**, 215601.
- 91 R. Y. N. Gengler, D. S. Badali, D. Zhang, K. Dimos, K. Spyrou, D. Gournis and D. Miller, Revealing the ultrafast process behind the photoreduction of graphene oxide, *Nat. Commun.*, 2013, **4**, 2560.
- 92 X. Zheng, B. Jia, H. Lin, L. Qiu, D. Li and M. Gu, Highly efficient and ultra-broadband graphene oxide ultrathin lenses with three dimensional subwavelength focusing, *Nat. Commun.*, 2015, **6**, 8433.
- 93 Y. Chen, *et al.*, Reduced Graphene Oxide Films with Ultrahigh Conductivity as Li-Ion Battery Current Collectors, *Nano Lett.*, 2016, **16**, 3616–3623.
- 94 G. Xin, *et al.*, Highly thermally conductive and mechanically strong graphene fibers, *Science*, 2015, **349**, 1083–1087.
- 95 D. Voiry, *et al.*, High-quality graphene via microwave reduction of solution-exfoliated graphene oxide, *Science*, 2016, aah3398, DOI: 10.1126/science.aah3398.
- 96 H. Feng, R. Cheng, X. Zhao, X. Duan and J. Li, A low-temperature method to produce highly reduced graphene oxide, *Nat. Commun.*, 2013, **4**, 1539.
- 97 A. Y. S. Eng, Z. Sofer, S. Huber, B. Daniel, M. Marysko and M. Pumera, Hydrogenated Graphenes by Birch Reduction: Influence of Electron and Proton Sources on Hydrogenation Efficiency, Magnetism, and Electrochemistry, *Chem. – Eur. J.*, 2015, **21**, 16828.